High-Resolution Elemental Mapping of Lunar Surface

Team 73

Inter IIT Techmeet 2024

Abstract

High-resolution elemental mapping of the Moon's surface is crucial to understand its geological evolution, identify the potential resources, and enhance future exploration missions. Using data from the **Chandrayaan- 2 Large Area Soft X-ray Spectrometer (CLASS)**, we developed a comprehensive framework to derive and visualize elemental ratio maps through X-ray fluorescence (XRF) spectroscopy. This research focuses on the primary elements forming rocks, specifically magnesium (Mg), aluminum (Al), silicon (Si), and calcium (Ca) as their line intensity ratios to reduce solar angle and flux variations effects.

A **dynamic pipeline** was developed to process the large dataset from XRF efficiently calculate elemental line fluxes and produce high-resolution, ratio-based compositional maps superimposed on lunar albedo maps. By employing advanced spectral modeling and overlapping track analysis, we achieved enhanced **sub-pixel spatial resolutions**, enabling the identification of fine-scale geochemical variations in the lunar crust. These **dynamic and interactive maps** provide critical insights into the Moon's compositional diversity, highlight resource-rich regions, and establish an innovative and scalable approach for planetary data analysis and visualization. This work lays a strong foundation for future lunar exploration and planetary geochemical studies.

1. Introduction

1.1. Background

The surface composition of the Moon, shaped by crustal materials, volcanic residues, and impact-generated ejecta, is valuable for inferences of planetary evolution and resource distribution. High-resolution elemental composition mapping is, therefore essential for understanding the Moon's geology and supporting lunar exploration missions. XRF spectroscopy, used by the CLASS instrument of Chandrayaan-2, detects characteristic XRF lines emitted by elements due to the solar excitation. This allows for detailed analysis of key rock-forming elements such as magnesium (Mg), aluminum (Al), silicon (Si), and calcium (Ca).

1.2. Significance

The CLASS data is used to identify and analyze XRF lines in spectra, which then determines the corresponding elements and their significance in lunar geology. By modeling the spectra, we quantify XRF line flux for each detected element, precisely calculating elemental ratios such as Mg/Si, Al/Si, and Ca/Si. These **ratios are mapped onto a lunar albedo base map**, such as the Lunar Reconnaissance Orbiter's Wide Angle Camera global map, to reveal compositional heterogeneity.

Uncertainties are derived for each calculation to enhance accuracy and ensure the robustness of the results. Overlapping orbital tracks are examined to achieve sub-pixel resolution and determine ratios that best capture terrain compositional diversity. This technique reveals fine-scale geochemical variations, which advances the understanding of crustal differentiation on the Moon, magmatic processes, and potential resource-rich regions.

High-resolution mapping with interactive visualization is of great help in lunar data analysis, providing actionable insights for future scientific, exploratory, and resource-utilization missions.

2. Advancing Lunar Surface Composition Analysis

Recent advancements in lunar exploration have greatly enhanced our understanding of the Moon's surface composition. Among the most ambitious goals of modern lunar science is the creation of high-resolution elemental maps that reveal the compositional diversity of the Moon's geological terrains. This study harnesses data from the CLASS instrument aboard Chandrayaan-2, which has been orbiting the Moon since 2019, detecting characteristic X-rays emitted by surface elements when excited by solar radiation. By analyzing this rich dataset, the study aims to provide unprecedented insights into the Moon's geology and resource potential through advanced mapping and visualization techniques.

The project focuses on utilizing CLASS data to calculate and map elemental ratios, with an emphasis on Mg/Si and Al/Si ratios. These ratios are critical indicators of key geological processes, such as magmatic differentiation and crustal evolution, enabling the **characterization of basaltic and feldspathic terrains**. Such an approach is vital for understanding the Moon's geological history, its compositional diversity, and potential resource deposits.

2.1. Cataloging XRF Line Detections:

A systematic analysis and cataloging of X-ray fluorescence (XRF) line detections for primary elements, such as magnesium, aluminum, and silicon. This involves recording the intensity and quality of each detection while accounting for variables like solar activity. The resulting catalog provides a robust dataset for further analysis and serves as a reference for future lunar missions.

2.2. Calculating Elemental Ratios:

Deriving elemental intensity ratios, such as Mg/Si and Al/Si, to minimize external influences like solar flare intensity

and incident angle. These ratios serve as reliable indicators of elemental composition, offering insights into geological processes such as volcanic activity, crustal differentiation, and regolith evolution.

2.3. High-Resolution Elemental Mapping:

Generating spatially resolved maps of elemental ratios overlaid on lunar albedo maps, such as those from the Lunar Reconnaissance Orbiter. These maps visually represent the distribution of elements and allow for correlations with geological features, demarcating compositional differences across terrains.

2.4. Interactive Visualization:

Developing dynamic, interactive maps to enable researchers to explore compositional data in greater detail. This interactive approach enhances understanding of the spatial relationships between compositional features and their geological contexts, fostering intuitive interpretations of the data.

2.5. Sub-Pixel Resolution Analysis:

Utilizing overlapping CLASS data from multiple orbits to achieve sub-pixel resolution, refining spatial details beyond the nominal resolution of the instrument. This allows for the identification of micro-structures, localized features, and subtle compositional variations, providing an unprecedented level of detail in lunar surface analysis.

2.6. Uncertainty Quantification:

Assessing uncertainties associated with XRF line detections and elemental ratios by analyzing variations in solar incidence angles, background noise, and detector sensitivity. This ensures the reliability of the derived maps and their scientific validity.

The study culminates in the identification of the most meaningful elemental ratios for geological analysis, the creation of high-resolution maps that **reveal compositional heterogeneity**, and the advancement of mapping techniques to achieve finer spatial resolution. These efforts contribute to a deeper understanding of the Moon's origin, evolution, and potential as a resource-rich celestial body, paving the way for future lunar exploration and resource utilization.

3. Literature Review

The Chandrayaan-2 Large Area Soft X-ray Spectrometer, or CLASS, represents a giant leap forward in the examination of lunar XRF. Since it was placed in orbit in September of 2019, CLASS has been gathering lunar X-ray spectra. Previous missions like Apollo and Lunar Prospector have demonstrated the value of such approaches in creating elemental maps, but CLASS extends this capability with higher spatial resolution and broader coverage, and **we aim to analyze the relative elemental ratios Mg/Si and Al/Si**, etc., and aim to enhance the resolution of lunar maps and derive the understanding of lunar crustal composition, geological evolution and identifying potential sites for in situ resource utilization. This report integrates relevant information obtained from various past missions and observations for arriving at the best possible solutions for the end-term deliverables.

3.1. Selection of high- quality spectral data:

To determine the threshold of the intensity of the peak to be set for selecting high-quality spectral data for elemental analysis during space observations, we discard intervals where there is significant distortion of the spectrum due to the interaction of particles. To achieve this, **we identify the spectral lines with intensities above 3σ from the nominal average background and free from particle contamination** as good intervals which can be considered under our observation for further analysis. This idea was inspired by the approach described in the research paper "Lunar elemental abundances as derived from Chandrayaan-2". This method is based on the concept that the spectral background is steady when the orbiter is on the night side, and a monthly average is taken as a reference background. Moreover, during geotail passes, there is a distortion in the background due to particle interaction, **introducing spectral lines such as of Al-Kα and Cu-Kα spectral lines with fluctuating intensity ratios**. So, the data intervals with significant spectral distortions due to particle interactions are not considered for spectral analysis and only the intensities exceeding three times the nominal background (3σ) and free from contamination are deemed suitable for spectral modeling. The hypothesis behind using this method is explained in detail under the section of Data Processing.

3.2. Three Sigma Criterion for Confidence-Based Signal Detection

The Three Sigma Criterion, also known as **the $\mu + 3\sigma$ criterion**, is a statistical model used to distinguish between true signals and background noise in spectral analysis. By employing measures such as the mean (μ) and standard deviation (σ), this approach identifies significant spectral peaks with high confidence and eliminates random noise.

- **Three-Sigma Criterion and Statistical Analysis:**
  We calculate the background mean (μ_{bg}) and standard deviation (σ_{bg}) for pre-defined individual elemental ranges. Peaks with intensity I_{peak} greater than $\mu_{bg}+3\sigma_{bg}$ are considered statistically significant, ruling out fluctuations as the cause.
- **Key Formulae for Noise Parameters:**
  - **Mean of the Background Intensity (μ_{bg}):**

    $$\mu_{bg} = \frac{1}{N}\sum_{i=1}^{N} I_{bg,i}$$

    where N is the total number of background intensity measurements and $I_{bg,i}$ is the intensity of the background in the i-th measurement.
  - **Background Intensity Standard Deviation (σ_{bg}):**

    $$\sigma_{bg} = \sqrt{\frac{1}{N-1}\sum_{i=1}^{N}(I_{bg,i} - \mu_{bg})^2}$$

- **Detection Threshold for Significant Peaks:**

$$I_{peak} > \mu_{bg} + 3\sigma_{bg}$$

- **Why 3σ Is the Desired Threshold:**
  - **Avoids False Positives:** The probability that noise exceeds the 3σ threshold is only 0.3
  - **Balances Sensitivity and Specificity:** Lower thresholds, such as 1σ, increase sensitivity but may lead to false positives, while higher thresholds, like 5σ, reduce false positives but might miss weaker true peaks.
- **Usage in Spectral Analysis:**
  - **Calculating Background Noise Parameters:** Noise parameters (μ_{bg} and σ_{bg}) are derived from noisier parts of the spectrum, often obtained during the night or in areas with weak signals.
  - **Identifying Significant Peaks:** Peaks with amplitudes larger than $\mu_{bg} + 3\sigma_{bg}$ are considered statistically valid. Signals from elements like Fe, Mg, or Al above this threshold and repeating over time are considered real.
  - **Noisy Data Elimination:** The Three-Sigma Criterion eliminates false positives due to instrumental artifacts (e.g., Al-K or Cu-K lines) or random fluctuations.
- **Three-Sigma Criterion Hypothesis Testing Framework:** The Three-Sigma Criterion can be integrated into hypothesis testing to classify a signal.
  - **Null Hypothesis (H_0):** The observed peak is noise:

$$I_{peak} \leq \mu_{bg} + 3\sigma_{bg}$$

  - **Alternative Hypothesis (H_1):** The observed peak represents a real signal:

$$I_{peak} > \mu_{bg} + 3\sigma_{bg}$$

  - **Test Statistic (Z):**

$$Z = \frac{I_{peak} - \mu_{bg}}{\sigma_{bg}}$$

    If $Z > 3$, reject H_0 and the signal is meaningful. If $Z \leq 3$, fail to reject H_0 and the signal may be noise.
- **Illustrative Computation:**
  For magnesium (Mg) in a spectral dataset:
  - $\mu_{bg} = 2{,}88$, $\sigma_{bg} = 0{,}05$
    Observed peak intensity: $I_{peak} = 7{,}37$
  - The test statistic is:

$$Z = \frac{7{,}37 - 2{,}88}{0{,}05} = 89{,}8$$

    Since $Z > 3$, the peak is statistically significant, corresponding to a genuine signal.
- **Importance of the Three-Sigma Criterion:**
  - **Consistency Across Elements:** The criterion delivers accurate results for various elements such as Fe, Mg, and Al, ensuring that actual signals are detected in diverse datasets.
  - **Sensitivity to Complex Spectral Environments:** If the background intensity is not normally distributed, advanced statistical methods can further refine μ_{bg} and σ_{bg} to improve robustness.
  - **High Confidence:** The Three-Sigma Criterion minimizes false positives while maintaining sensitivity, ensuring high-quality, scientifically valid datasets.

3.3. Comparative analysis of elemental ratios in different regions:

A key part of this study is the comparative analysis of elemental ratios in different lunar regions. Using elemental maps of Mg, Al, Si, and Fe, generated from 2,458 CLASS footprints with a spatial resolution of 150 x 12.5 km, we analyze compositional differences between the Moon's mare and highland regions. Mg and Al line intensities are used as indicators for distinguishing these regions. The elemental ratios, specifically Mg/Si and Al/Si, provide insights into the composition of different lunar areas.

Previous studies have shown that mare regions are rich in Magnesium and Iron, while highland regions tend to be Aluminum-rich. However, the Silicon map does not show a distinct boundary between mare and highland regions. This highlights the complex and heterogeneous nature of the lunar surface.

Further analysis of specific lunar sub-regions, such as **Oceanus Procellarum and Mare Imbrium**, reveals notable variations in Mg abundance, suggesting diverse magmatic sources. The **Mg abundance is higher in these regions due to the presence of different basaltic magmas**. In contrast, **Mare Frigoris and Mare Serenitatis show localized areas with higher Mg relative to Al, indicating less-evolved, primitive basalts**. The variability in Mg abundance can be quantified by computing the standard deviation of the Mg concentrations in these areas:

$$\sigma_{Mg} = \sqrt{\frac{1}{N}\sum_{i=1}^{N}(Mg_i - \mu_{Mg})^2}$$

The broader range of Mg concentrations in mare regions contrasts with the narrow range observed in the farside highlands. Additionally, the South Pole-Aitken Basin, despite being a basin feature, shows Mg abundances comparable to those in Oceanus Procellarum, likely due to the excavation of mantle materials. This comparative analysis of elemental ratios offers critical insights into the geological processes that have shaped the Moon's surface.

3.4. XSM Data Analysis:

The Solar X-ray Monitor (XSM) is a crucial component for enhancing the accuracy of lunar XRF measurements. The XSM generates raw (level-1) and calibrated (level-2) data files. Raw files include .fits, .hk, and .sa files, while calibrated files, such as .gti, .pha, and .lc files, contain processed data that is ready for analysis. The Light Curve (.lc) files store time-series data representing photon count rates over time, providing a temporal resolution of 1 second and covering the energy range of 1–15 keV.

The use of .lc files enables time-resolved analysis, making it easier to examine variations in solar X-ray emission. These files also contain pre-processed data that accounts for variations in the effective area, making them compatible with visualization tools. Moreover, the information in these files is essential for correcting solar flux during XRF measurements.

Where $\text{Flux}_{\text{observed}}$ is the observed solar flux, and **the *Effective Area Correction* accounts for variations in the instrument's effective area**. By incorporating XSM data into the analysis, we can account for solar flux fluctuations, significantly improving the precision of the XRF measurements and elemental composition analysis.

3.5. Database selection:

MySQL, which is a relational database management system and is widely known for being used in managing structured data in scientific and exploratory pipelines, is integrated with our backend pipeline as our database. Its integration with Python libraries like **mysql-connector-python** simplifies data ingestion, transformation, and export to external analysis tools such as Pandas or NumPy. In geospatial analysis, as in our case, relational databases allow us seamless integration of spatial data with compositional metrics, enabling fast querying and updating results, as required in our workflow pipeline. Usage of MySQL as our database makes our pipeline dynamic and robust for data extraction, updation, and storage, along with implementing other methodologies.

Operation	Using CSV (in s)	Using MySQL (in s)	Remarks
Data Reading	0.05	0.01	MySQL parsing overhead dominates here, even for small files
Preprocessing	0.15	0.15	Includes, .fits calibration and adjustments where time remains constant.
Data Updation	1	0.025	CSV requires rewriting the file, whereas MySQL performs direct updates efficiently.
Refreshing Heatmap	0.25	0.04	CSV involves re-parsing the updated file, whereas MySQL uses indexed queries.
End-to-End Processing	0.65	0.23	Significant reduction due to MySQL's optimized operations.

Figura 1: Comparison between SQL and CSV data formats

4. Methodology for Deliverables

This methodology outlines a structured, detailed approach for mapping and analyzing lunar elemental compositions to achieve scientifically accurate and visually engaging results. It comprises multiple phases, starting from raw data preprocessing and progressing through advanced data analysis, interpolation, and visualization techniques. Each phase is designed to ensure that the final outcomes not only meet high standards of scientific accuracy but also provide a user-friendly platform for further research and exploration.

4.1. Data Preprocessing

The foundation of any accurate analysis lies in properly preprocessing raw data. Lunar spectral data often contains noise, inconsistencies, and environmental influences such as solar flares, which require careful attention before further analysis.

4.1.1. Cleaning and Calibration

- **Noise Reduction:** Raw data is cleaned to remove background noise that could obscure elemental peaks or introduce inaccuracies. This step ensures that the detected signals correspond only to the lunar surface's composition.

- **Solar Flare Corrections:** High-energy solar flares can distort the readings of certain elements. Adjustments are made using **XSM solar flare data to account for these distortions**. By identifying intervals of high and low solar flare activity, corrections are applied to accurately represent elements that require more energy for photon excitation.

- **Power Law Continuum Adjustments:** To further mitigate flare-induced distortions, a power-law continuum is applied, which smooths out irregularities and improves the reliability of detected element intensities. The corrected intensity is given by:

$$I_{\text{adjusted}}(E) = I_{\text{measured}}(E) - P(E)$$

where $I_{\text{adjusted}}(E)$ is the corrected intensity, $I_{\text{measured}}(E)$ is the observed intensity, and $P(E)$ is the power-law continuum.

4.1.2. Solar Angle-Based Classification

- Data is categorized based on the solar angle, dividing it into dayside and nightside datasets.

- The sunlight's influence on the lunar surface varies between these regions, and classification ensures that only relevant data is utilized in subsequent stages. **This segmentation improves the accuracy of value calibration and allows for reliable comparisons between energy and count values.**

4.2. Elemental Peak Identification

Accurately identifying the energy peaks corresponding to different elements is crucial for determining the Moon's elemental composition.

4.2.1. Defining Energy Ranges

- Spectral data is analyzed to define energy ranges associated with specific elements. These ranges are determined based on known elemental signatures, ensuring precision in isolating peaks.
- Filtering techniques are applied to exclude irrelevant data and focus on key features within the spectral graph.

4.2.2. Hypothesis Testing Using Gaussian Distribution

- Once peaks are identified, Gaussian distribution-based hypothesis testing is employed to confirm their authenticity.
- The Gaussian distribution is represented as:

$$f(x) = a \cdot e^{-\frac{(x-\mu)^2}{2\sigma^2}}$$

  where a is the amplitude of the peak, μ is the mean energy value, and σ is the standard deviation.
- Hypothesis testing validates peaks corresponding to elements with statistical significance p <0.05.

4.3. Mapping Lunar Elemental Ratios

Mapping the elemental ratios involves aligning spatial data with lunar coordinates, interpolating missing values, and creating interactive visualizations to explore the Moon's geological diversity.

4.3.1. Spatial Data Alignment

- Georeferencing: Elemental data is georeferenced to precise lunar coordinates, ensuring that each data point represents its actual location on the lunar surface.
- Grid Construction: A uniform grid is constructed using centroid methods. The centroid C for a region is given by:

$$C_x = \frac{\sum_{i=1}^{n} x_i \cdot w_i}{\sum_{i=1}^{n} w_i}, \quad C_y = \frac{\sum_{i=1}^{n} y_i \cdot w_i}{\sum_{i=1}^{n} w_i}$$

  where (x_i, y_i) are coordinates, and w_i represents weights (e.g., intensity values).

4.3.2. Interpolation with Kriging

- Kriging interpolation is employed to fill gaps in the data, creating smooth and continuous spatial representations of elemental ratios. The Kriging estimator is:

$$\hat{Z}(s) = \sum_{i=1}^{n} \lambda_i \cdot Z(s_i)$$

  where $\hat{Z}(s)$ is the estimated value at location s, $Z(s_i)$ are known values, and λ_i are weights minimizing variance.

4.3.3. Dynamic Interactive Maps

- Base Map Creation: Maps are built on a lunar albedo base map.
- Features: Interactive maps support panning, zooming, and overlaying information. Automatic updates enable real-time data integration.

4.4. Identification of Optimal Elemental Ratios

Optimizing elemental ratios helps distinguish compositional differences between lunar regions. Ratios such as Al/Si, Mg/Si, and Ca/Si are analyzed for geological relevance. A custom optimization algorithm maximizes contrast in compositional differences. The objective function is:

$$J = \sum_{i=1}^{n} \frac{(R_{i,\text{region1}} - R_{i,\text{region2}})^2}{\sigma_i^2}$$

where $R_{i,\text{region1}}$ and $R_{i,\text{region2}}$ are ratios in regions, and σ_i is the standard deviation.

For Fine-Scale Mapping with Sub-Pixel Resolution we have implemented advanced kriging interpolation techniques create sub-pixel resolution maps. These maps reveal fine-scale geological features, enabling detailed analysis.

The integration of processed data, optimized ratios, and high-resolution maps culminates in a robust analytical framework for lunar exploration.

5. Surface Analysis and Resource Identification

5.1. Data Comparison and Selection

- **Raw Data:** Unprocessed and prone to noise and inconsistencies.
- **Grid Data:** Spatially structured but exhibits variability based on processing methods.
- **Kriged Data:** Statistically interpolated, addressing spatial inconsistencies, and demonstrating the least deviation from the LPGRS reference, making it the most reliable dataset for further analysis.

We observed that the kriged data provided a robust foundation, reducing deviation and enhancing the reliability of conclusions.

5.2. Analysis and Results

5.2.1. Mare and Highlands Classification

Dynamic Threshold-Based Classification:

- **Threshold Percentiles:** Explored combinations of high (20th–80th) and low (10th–70th) thresholds for Al/Si and Mg/Si ratios.
- **Classification Logic:**
  - **Highland Regions:** Identified by high Al/Si and low Mg/Si ratios.
  - **Mare Regions:** Marked by low Al/Si and high Mg/Si ratios.
- **Spatial Labeling:** Mapped using latitude and longitude coordinates with dynamic threshold combinations.
- **Fixed Regional Definitions:** Predefined geographical regions (e.g., Mare Tranquillitatis, Oceanus Procellarum) were used for precise validation.

Outcomes:

- **Scientific Insights:** Confirmed known mare regions (e.g., Mare Tranquillitatis) with high Mg/Si ratios and highlands with anorthositic compositions.
- **Validation:** Dynamically classified regions aligned closely with predefined geographical regions.

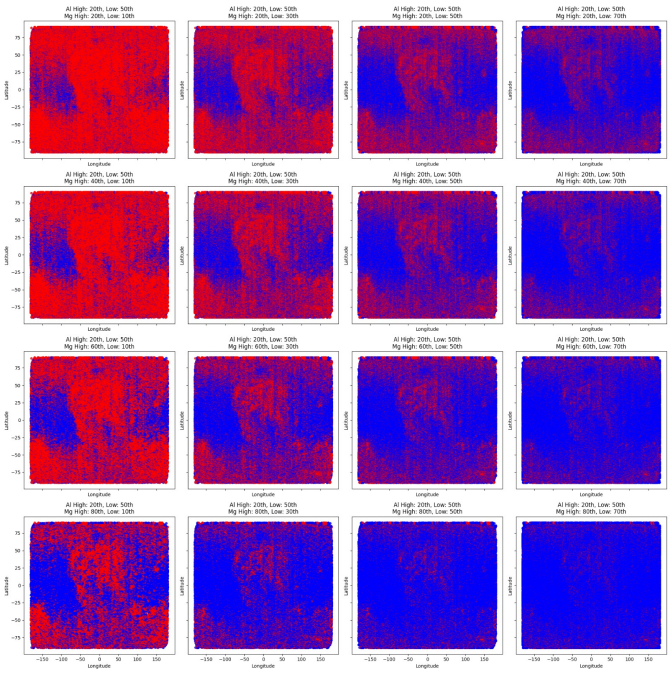

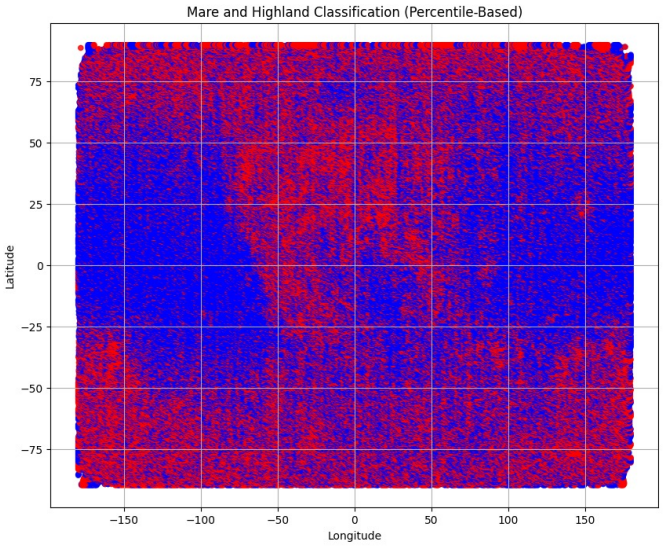

5.2.2. Regional Analysis

Conducted for key regions, including Mare Imbrium and Australe, using elemental ratios (Al/Si, Mg/Si, Ti/Si, etc.) for compositional and geological profiling.

Outcomes:

- **Mare Imbrium:** High variability in Mg/Si and Ti/Si ratios indicated complex volcanic activity.
- **Australe:** Low variability suggested stable terrain, supporting hypotheses of water-ice deposits.
- **Other Regions:** Highlighted ISRU potential in mare regions like Oceanus Procellarum and stability in highland areas.

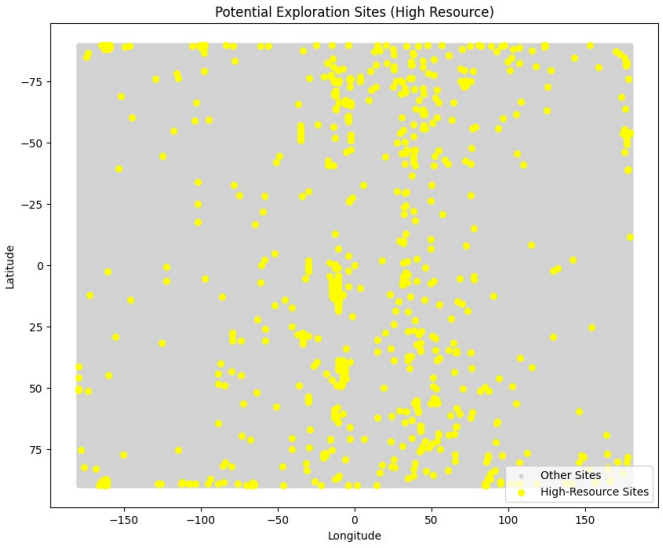

5.2.3. Water Indicators

Analysis: Used low Mg/Si and Fe/Si ratios (1st percentile) to identify potential water-ice reservoirs.

Outcome: Highland and polar regions were highlighted as potential sites for water retention, paving the way for future research into lunar water resources.

5.2.4. Indicators of Volcanic Activity

Threshold: High Ti/Si ratios (95th percentile) indicated titanium-rich basalts, typical of volcanic regions.

Outcome: Identified volcanic hotspots in Oceanus Procellarum and Mare Tranquillitatis, providing insights into lunar thermal history.

5.2.5. Impact Features

Ratios: Elevated **Fe/Si (75th percentile)** and **Cr/Si (95th percentile)** were used to detect meteoritic impact sites.

Outcome: Confirmed known impact sites and identified new potential sites, enriching our understanding of lunar bombardment history.

5.2.6. ISRU Ore Deposits

Thresholds:

- High Mg/Si (75th percentile), Fe/Si (75th percentile), and Ti/Si (95th percentile) for identifying resource-rich regions.

Outcome: Hotspots in Mare Imbrium and Oceanus Procellarum were mapped as prime candidates for ISRU potential.

5.2.7. Sub-Pixel Resolution Enhancement

Methodology: Transitioned from a resolution of $0{,}4^\circ \times 0{,}4^\circ$ to $0{,}1^\circ \times 0{,}1^\circ$ using Weighted Overlap Averaging.

Equation:

$$\text{Updated Value} = \frac{n \cdot \text{Previous Value} + \text{New Patch Value}}{n+1}$$

Where n is the number of overlapping patches contributing to a grid cell.

Strengths: Improved accuracy and fidelity in mapping overlapping data patches.

Outcome: Created high-resolution grids revealing subtle geological variations and providing a more detailed lunar surface analysis.

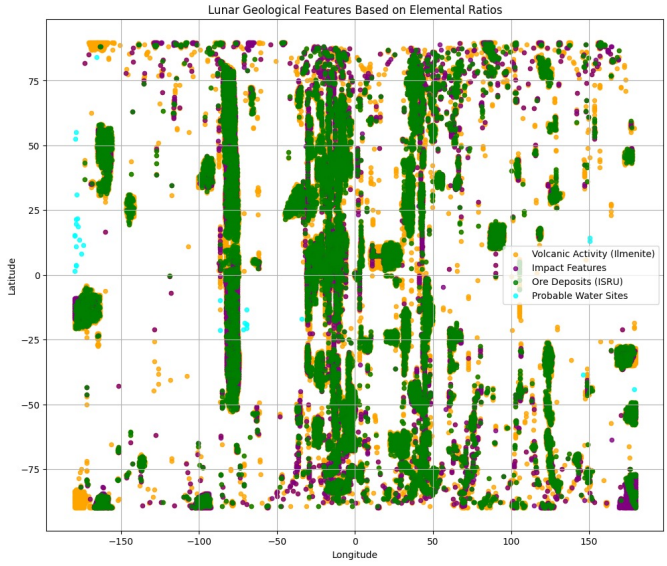

5.3. Overall Insights

The comprehensive analyses provided insights into lunar geography, geological history, and resource potential, emphasizing:

- Robust classification methods for compositional regions.
- Enhanced resolution techniques for precise mapping.
- Strategic identification of ISRU opportunities and water-ice indicators, crucial for sustainable lunar exploration.

6. Future Aspects

The detailed surface analysis and resource identification methodologies outlined above pave the way for numerous future research directions and advancements. By leveraging the comprehensive insights gained from the analyses, several promising avenues can be explored to expand our understanding of the Moon and optimize its exploration and resource utilization. The following are the key aspects for future work, broken down into thematic areas:

1. **Targeted Lunar Exploration with Cataloging and Visualization using our pipeline**
   Our robust pipeline utilizes **MySQL**, **Neo4j**, and **Power BI** to facilitate targeted experiments on the lunar surface. By leveraging geospatial data inputs (latitude and longitude), our pipeline provides actionable insights, including elemental abundance ratios, probabilities of water presence, volcanic activity indicators, and other features. These insights allow us to plan missions with precision and optimize the deployment of lunar rovers for scientific experiments. By inputting geospatial coordinates, our system retrieves all relevant data—including elemental compositions, water probabilities, volcanic activity, and ore deposits—**for a specified region of 12.5 km X 12.5 km**, enabling a comprehensive analysis of lunar surface characteristics to guide mission objectives effectively.

2. **Enhancing Data Resolution and Precision**

   - **Advanced Interpolation Techniques:** The transition from $0{,}4^\circ \times 0{,}4^\circ$ to $0{,}1^\circ \times 0{,}1^\circ$ resolution using Weighted Overlap Averaging has demonstrated significant improvements in spatial data fidelity.

     Future work can explore:

     - Incorporating machine learning-based interpolation techniques, such as Gaussian Processes, to further refine sub-pixel accuracy.
     - Utilizing ensemble methods to cross-validate and optimize interpolation outputs.

   - **Higher-Resolution Mapping:** Current methods rely on weighted averaging within predefined grid cells. The integration of satellite missions equipped with advanced spectrometers (e.g., high-resolution XRF or hyperspectral imaging) can provide finer datasets to reduce reliance on interpolation methods.

- **Dynamic Updating of Maps:** As new data becomes available from upcoming lunar missions, dynamic methods can be developed to seamlessly integrate fresh datasets into existing high-resolution maps, ensuring up-to-date and accurate compositional representations.

3. **Refining Compositional and Geospatial Analyses**
   - **Dynamic Classification Thresholds:**
     - Expanding on the flexibility provided by percentile-based thresholds, future research can incorporate adaptive thresholding algorithms that automatically adjust based on regional trends or specific research objectives.
     - Integration of **Bayesian approaches** to refine classification probabilities based on prior knowledge and observed data trends.
   - **Enhanced Spatial Labeling:** Develop real-time spatial classification systems that account for temporal variations in lunar surface data (e.g., temperature-dependent compositional changes or regolith redistribution from impacts).
   - **Incorporating Multi-Modal Data:**
     - Combine geochemical data (e.g., Al/Si, Mg/Si ratios) with topographical, thermal, and seismic datasets to create multi-layered, context-aware maps.
     - Cross-reference lunar data with meteoritic composition databases to improve the accuracy of impact site identification.
4. **Exploring Resource Utilization Potential**
   - **ISRU (In-Situ Resource Utilization) Opportunities:**
     - The identified hotspots in **Mare Imbrium** and **Oceanus Procellarum** provide a strong starting point for resource extraction studies. Future work should focus on:
       - Detailed feasibility studies of resource extraction, including the energy and equipment requirements for mining titanium and magnesium-rich basaltic regions.
       - Simulation of oxygen extraction from ilmenite (titanium ore) and quantifying the efficiency under varying environmental conditions.
   - **Water-Ice Prospecting:**
     - **Highland and polar regions** highlighted as potential water reservoirs warrant detailed exploration to confirm ice presence and estimate volume.
     - Future missions equipped with ground-penetrating radar or neutron spectrometers can validate the hypothesis of ice deposits, refining models for extraction and usage in life support systems.
5. **Investigating Lunar Geological Evolution**
   - **Volcanic Activity and Thermal History:**
     - High Ti/Si regions indicating volcanic activity provide insights into the Moon's thermal evolution. Future studies can:
       - Utilize thermodynamic models to simulate past lava flows and their chemical differentiation.
       - Analyze isotopic compositions (e.g., titanium isotopes) to estimate the age of volcanic activity.
   - **Impact Event Chronology:**
     - The identified impact features with high Fe/Si and Cr/Si ratios allow for a detailed reconstruction of lunar bombardment history.
     - Dating techniques such as **crater counting or isotopic dating** of impact ejecta should be employed to establish a timeline of major meteoritic events.
6. **Advancing Water and Life-Support Systems**
   - **Sustainable Exploration Framework:**
     - The identified water-rich regions can support the establishment of lunar bases. Future research should focus on:
       - Designing water **extraction technologies**, such as **sublimation-based techniques**, for icy regolith.
       - Integrating ISRU-derived water into closed-loop life support systems for human habitation.
   - **Biological Suitability:** Evaluate the compatibility of lunar materials with biological systems to determine feasibility for agriculture and habitation.
7. **Technological Innovations in Data Processing**
   - **Machine Learning for Lunar Data Analysis:**
     - Use deep learning models to classify regions dynamically, reducing manual threshold selection and improving classification accuracy.
     - Employ **unsupervised clustering algorithms** to identify previously unknown compositional or geological features.
   - **Real-Time Processing Pipelines: Develop onboard processing systems** for lunar missions to analyze data in real time and reduce the dependency on Earth-based analysis.
8. **Supporting Future Missions**
   - **Collaborations with Upcoming Lunar Missions:**
     - Aligning methodologies with ISRO's Chandrayaan missions to leverage synergies in data collection and analysis.
     - Contributing insights to global lunar resource maps to guide mission planning and resource prioritization.
   - **Long-Term Vision:** The methodologies and results presented can form the foundation for a lunar resource atlas, a globally accessible database guiding both scientific research and commercial activities on the Moon.

Referencias

[1] S. Narendranath, N. S. Pillai, M. Bhatt, K. Vadodariya, R. Vatedka, S. P. Tadepalli, A. Sarwade, A. Tyagi, V. Sharan, *Lunar elemental abundances as derived from Chandrayaan-2*, Icarus, vol. 410, pp. 115898, 2024. doi:10.1016/j.icarus.2023.115898.

[2] S. Narendranath, P. S. Athiray, P. Sreekumar, R. Vatedka, A. Tyagi, B. J. Kellett, and the CLASS team, *Mapping lunar surface chemistry: New prospects with the Chandrayaan-2 Large Area Soft X-ray Spectrometer (CLASS)*, Advances in Space Research, vol. 54, no. 10, pp. 1993-1999, 2014. doi:10.1016/j.asr.2013.04.008.

[3] P. S. Athiray, S. Narendranath, P. Sreekumar, S. K. Dash, B. R. S. Babu, *Validation of methodology to derive elemental abundances from X-ray observations on Chandrayaan-1*, Planetary and Space Science, vol. 75, pp. 188-194, 2013. doi:10.1016/j.pss.2012.10.003.

[4] N. S. Pillai, S. Narendranath, K. Vadodariya, S. P. Tadepalli, et al., *Chandrayaan-2 Large Area Soft X-ray Spectrometer (CLASS): Calibration, In-flight performance and first results*, Icarus, vol. 363, pp. 114436, 2021. doi:10.1016/j.icarus.2021.114436.

[5] R. K. Sinha, V. Sivaprahasam, M. Bhatt, et al., *Geological characterization of Chandrayaan-2 landing site in the southern high latitudes of the Moon*, Icarus, vol. 337, pp. 113449, 2020. doi:10.1016/j.icarus.2019.113449.

[6] A. J. Gloudemans, E. Kuulkers, R. Campana, et al., *Re-evaluation of Lunar X-ray observations by Apollo 15 and 16*, Astronomy & Astrophysics, vol. 649, A174, 2021. doi:10.1051/0004-6361/202140321.

[7] M. Shanmugam, S. V. Vadawale, A. R. Patel, et al., *Alpha Particle X-Ray Spectrometer (APXS) On-board Chandrayaan-2 Rover – Pragyan*, arXiv, 2019.arXiv:1910.09232.

[8] F. Zaman, L. W. Townsend, W. C. de Wet, et al., *Composition variations of major lunar elements: Possible impacts on lunar albedo spectra*, Icarus, vol. 369, pp. 114629, 2021. doi:10.1016/j.icarus.2021.114629.

[9] R. C. Elphic, D. J. Lawrence, W. C. Feldman, et al., *Lunar rare earth element distribution and ramifications for FeO and TiO2*, Journal of Geophysical Research: Planets, vol. 105, no. E8, pp. 20333-20345, 2000. doi:10.1029/1999JE001176.

[10] O. Gasnault, C. d'Uston, W. C. Feldman, et al., *Lunar fast neutron leakage flux calculation and its elemental abundance dependence*, Journal of Geophysical Research: Planets, vol. 105, no. E2, pp. 4263-4271, 2000. doi:10.1029/1999JE001124.

[11] N. Hasebe, N. Yamashita, O. Okudaira, et al., *The high precision gamma-ray spectrometer for lunar polar orbiter SELENE*, Advances in Space Research, vol. 42, no. 2, pp. 323-330, 2008. doi:10.1016/j.asr.2007.05.046.

[12] A. L. Turkevich, *Average chemical composition of the lunar surface*, The Moon, vol. 8, no. 3, pp. 365-367, 1973.

[13] J. K. Wilson, H. E. Spence, N. A. Schwadron, et al., *Precise detections of solar particle events and a new view of the moon*, Geophysical Research Letters, vol. 47, no. 1, pp. e2019GL085522, 2020.

[14] F. A. Zaman, L. W. Townsend, W. C. de Wet, et al., *Modeling the Lunar Radiation Environment*, Space Weather, vol. 20, no. 8, pp. e2021SW002895, 2021. doi:10.1029/2021SW002895.

[15] K. Yumoto, Y. Cho, J. A. Ogura, et al., *Elemental analyses of lunar soils using laser-induced breakdown spectroscopy*, Spectrochimica Acta Part B, vol. 221, pp. 107049, 2024. doi:10.1016/j.sab.2024.107049.

[16] H. Nagaoka, M. Ohtake, Y. Karouji, et al., *Studies of lunar crust using Kaguya observations*, Icarus, vol. 392, pp. 115370, 2023.

[17] A. S. Laxmiprasad, R. V. L. N. Sridhar, A. Goswami, et al., *Laser Induced Breakdown Spectroscope on Chandrayaan-2 Rover*, Current Science, vol. 118, no. 4, pp. 573-581, 2020.

[18] L. Zhang, Y. Yang, Z. M. Chen, et al., *Elemental compositions of lunar plagioclase: Chang'e 5 insights*, Icarus, vol. 413, pp. 116002, 2024.

[19] S. Narendranath, P. S. Athiray, P. Sreekumar, et al., *Lunar X-ray fluorescence observations by Chandrayaan-1*, Icarus, vol. 214, no. 1, pp. 53-66, 2011.